Activated Radiationless Decay of Rhodamine 3B: Polarity and Friction Effects

José A. B. Ferreira,[†] Sílvia M. B. Costa,*[,†] and L. F. Vieira Ferreira[‡]

Centro de Química Estrutural, Complexo I, Instituto Superior Técnico, Av. Rovisco Pais 1, 1049−001 Lisboa, Portugal, and Centro de Química-Física Molecular, Complexo I, Instituto Superior Técnico, Av. Rovisco Pais 1, 1049−001 Lisboa, Portugal

Received: May 11, 2000; In Final Form: October 3, 2000

The intramolecular activated nonradiative decay of the first excited singlet of the Rhodamine 3B cation is studied in a large number of polar solvents covering a wide range of viscosities. The photophysics are interpreted in terms of an isomerization process occurring at the diethyl amino group with adiabatic barrier crossing. The experimental data show that friction effects determine the reaction rates, which are modeled in the framework of Kramers and Grote−Hynes theories. The reactant well wavenumber ($\omega_0/2\pi c$) is estimated as 30 cm^{-1} and coincides with the wavenumber of the barrier top ($\omega_b/2\pi c$) for the less viscous solvents. The former value is invariant with the solvent and is a good approximation to the reactive molecular mode involved in the nonradiative deactivation. The increase in dipole moment at the barrier top relative to the bottom of the reactant well is inferred from intrinsic barrier heights whose stabilization energies vary according to Onsager's theory of dielectrics.

1. Introduction

The photophysics of rhodamines (Rh) has been extensively studied since wide applications of these compounds are known and spread over different fields, namely as laser dyes,[1] as concentrators[2] in solar energy technology, also as specific probes of industrial and biochemical relevance[3] and, recently, their single molecule fluorescence has been studied.[4]

The group most widely studied of rhodamine molecules is the 9 − carboxyphenyl − Rh (Figure 1). They may exist in different molecular forms, e.g., lactone, zwitterion, acid, and also as ester. The former three nonesterified forms exist in equilibria depending on the polarity and proticity of the medium. In nonprotic low polarity media, nonesterified 9-carboxyphenyl-Rh exist as an equilibrium of lactone and zwitterionic forms. If the medium is protic, the acid form is also present.[5] These equilibria do not occur with esterified compounds. Thus, in polar solution, the molecular species is the cation although in weakly polar media the dyes exist preferentially as associated ion-pairs.[6]

Rhodamines have very low yields of intersystem crossing[1,5−8] and are generally highly fluorescent compounds. Different substitution patterns at the xanthene ring lead however to different photophysical behavior[1]. The fluorescence quantum yields of Rhodamine 6G (Rh6G) and Rhodamine 101 (Rh101) are identical, close to unity, and nearly temperature and solvent independent.[1,9] However, their structures are quite different as it is shown in Figure 1. Both molecules have a rotating 9-carboxyphenyl group. Consequently, this mechanism does not act as a deactivating pathway[10] for the first excited singlet state as it is generally observed for the non oxygen bridged analogue molecules, the triphenylmethane dyes (TPM). The main difference between the former two dyes lies in the substitution of the amino groups. Rhodamine 101 (Rh101) has the nitrogen atoms rigidly linked to the xanthene skeleton, whereas Rhodamine 6G (Rh6G) has free amine nitrogen secondary substituents with only one alkyl group. By contrast, 9-carboxyphenyl-Rh with di-alkylated nitrogen atoms nonlinked to the xanthene skeleton, as in Rhodamine B (RhB) have fluorescence quantum yields which are temperature, viscosity, and polarity dependent. However, at low temperatures[11] its fluorescence quantum yield is close to unity reaching a value similar to the one observed for the former two rhodamine molecules. From the photophysical comparison of the several classes of rhodamines, it is obvious that the mobility of the di-alkyl amino groups is involved in the activated nonradiative pathways of acid and ester 9-carboxyphenyl-Rh, as it has been suggested earlier.[1] However, it must be taken into consideration that the absence of one alkyl group from the nitrogen atoms changes completely the photophysics, slowing drastically the activated nonradiative process. In fact, this is the situation of Rh6G with secondary amine groups and of Rh123, with two primary amine groups. Similar findings were obtained concerning the substitution effect of nitrogen atoms made in the so-called TICT (twisted intramolecular charge transfer) molecules, such as DMABN (p-dimethyl amino benzonitrile), which undergo the formation of a second emissive state from the local excited state. The molecules MABN (*p*-methyl amino benzonitrile) and ABN (amino benzonitrile) do not show the characteristic dual emission.[12] No dual fluorescence has been observed in rhodamines either, and the answer to the

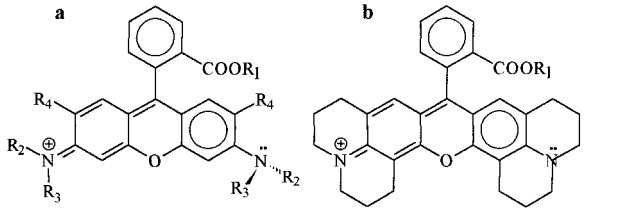

Figure 1. Molecular structures of some rhodamine cationic forms: a: Rhodamine 3B (ester): R_{1-3}=C_2H_5, R_4=H; Rhodamine B (acid form): R_1=H, R_{2-3}=C_2H_5, R_4=H; Rhodamine 6G (ester): $R_{1,3}$=C_2H_5, R_2=H, R_4=CH_3; b: Rhodamine 101 (acid form): R_1=H.

* To whom correspondence must be addressed. E-mail: sbcosta@popsrv.ist.utl.pt. Fax: (351) 218464455/7.

† Centro de Química Estrutural, Complexo I, Instituto Superior Técnico.

‡ Centro de Química-Física Molecular, Complexo I, Instituto Superior Técnico.

10.1021/jp0017543 CCC: $19.00
Published on Web 12/05/2000

problem of media induced fluorescence quantum yield variations may be found in the occurrence of isomerization and charge-transfer mechanisms. Using the TICT hypothesis,[13] invoked to explain the dual fluorescence in DMABN and similar compounds, the formation of a nonemissive biradicaloid charge transfer state was suggested as responsible for the observed activated fluorescence quenching in rhodamines.[14] The yield of formation of this state would depend mainly on intramolecular donor/acceptor ability.[15] An obvious consequence of the postulation of such model would be the dependence of the activated nonradiative rates on solvent viscosity and polarity. Higher rates would be expected in the less viscous solvents and in the more polar ones. On one hand, intramolecular rotation will be less hindered by the solvent drag and on the other hand, the new formed charge transfer state will be more stabilized by the field of solvent dipoles. The influence of the solvent role in the deactivating process was differently interpreted by Arbeloa et al. who have proposed a specific promoting mode for the thermally activated quenching of fluorescence in rhodamine dyes.[16−18] The role of the energy gap between electronic states involved[19] as well as electron transfer[20] were also invoked. The participation of a high triplet state to account for the deactivation pathway[21] was also postulated. A common feature, in all models referred to, is the participation of an intramolecular charge-transfer process.

The first quantitative attempt to study the dynamic nature of the activated intramolecular fluorescence decay in a rhodamine molecule was made by Tredwell and Osborne.[22] They studied the dye *N*-(2-tolyl)-*N*′-(2-tolyl-5-sulfonate)-rhodamine (FAV-2R) in protic solvents namely alkanols, water, and polyols. This molecule has a very short-lived (a few picoseconds) singlet excited-state whose lifetime increases with the viscosity of the medium. Thus, these authors interpreted the solvent and temperature changes of the fluorescence lifetime as a viscosity-dependent isomerization process occurring at the substituted amino group. The rate constants of this process were studied in the framework of Kramers' theory.[23]

In this paper, we report the study of thermally activated nonradiative decay of first excited singlet state of Rhodamine 3B (Rh3B) in polar protic and aprotic solvents with the aim of contributing to a further elucidation on the nature of this pathway. The dependence of solvent and of temperature on the activated part of the nonradiative rate constants, k_{nr}, are studied and interpreted in terms of two main contributions: polarity and friction. Both effects are included in the framework of Kramers[23] and Grote−Hynes[24] theories that are used to model the experimental data.

The structure of the paper is as follows: The experimental details are outlined in Section 2. Section 3 presents the experimental results on the photophysics of Rh 3B. Section 4 is dedicated to the modelization of experimental data, which is discussed in Section 5, and Section 6 contains the main conclusions of this work.

2. Experimental Section

2.1 Materials. Rhodamine 3B perchlorate (Radiant Dyes Chemie, Laser grade) was used as received. Water was twice distilled over quartz. The alcohols used were as follows: spectrophotometric grade ethanol (Merck) and glycerol (Aldrich); methanol for analysis (Merck), 1-propanol, 2-propanol, 1-butanol, 2-butanol, and 1-hexanol; spectroscopic grade. (Merck) 1,4-butanediol, 1,5-pentanediol and 2-methyl-2-propanol, 1-decanol (Fluka), 1,3-propanediol (BDH), tetraethyleneglycol (Fluka) and cyclohexanol (Eastman Kodak). Acetonitrile and formamide were Merck UVASOL solvents, and triacetine was purchased from Fluka. All of the alcohols were used as received. 1,2-ethanediol (Fluka) and propylene carbonate (Merck) were dried by column chromatography over silica gel (Merck). In all cases, the purity was checked by the absorption and fluorescence spectra in the UV−vis range.

2.2 Sample Preparation. All samples were prepared from an initial Rhodamine 3B ethanol stock solution from which an aliquot was taken to different flasks. The original ethanol was evaporated until dryness using a stream of nitrogen. The Rh3B concentration was kept at the low (to avoid aggregation and self-absorption/reemission effects) constant value of 6.8×10^{-7} M by addition of the given amount of each solvent. The samples were kept for 24 h and protected from light before the experimental measurements.

2.3 Apparatus. In both steady state and transient state measurements, 10-mm quartz rectangular cells were used, and the temperature was controlled within ±1 K using a circulating water stream on the apparatus cell holders. Absorption spectra were recorded with a Jasco V-560 UV/Vis spectrophotometer with blank correction. Emission spectra were recorded with a Perkin-Elmer MPF-3 spectrofluorimeter, and also with a Perkin-Elmer LS-50B, respectively described in refs 25a and 25b. The fluorescence quantum yields of Rh3B were measured using Rh6G (Cl^-) in ethanol solution as a reference.[26] The excitation was selected at 516 nm, keeping the optical density at this wavelength below 0.02. Integration of the corrected emission spectra was made over the emission wavelength range and corrections for changes in the respective refractive indexes were made according to Parker.[27] The steady-state measurements were made at $T = 296$ K.

Fluorescence decays were obtained using the time-correlated single photon counting technique with a PTI LS-100 equipment from Photon Technology International, described elsewhere[25a] (as well as fluorescence lifetime recovery procedure). The excitation source came from a discharge compartment filled with hydrogen at a relative pressure of −17 in. Hg. The excitation was selected at 540 nm and the emission collected at 585 nm. The fluorescence decays could be fitted with a single exponential. The quality of the fits was controlled by means of usual statistical parameters[28] namely χ^2 (1.1−1.2), DW (1.7−1.8), and runs test Z (around 0.5), as well as by visual inspection of the residuals and their autocorrelation functions.

3. Results

3.1 Rate Constants: Solvent and Temperature Dependence. *3.1.1 Fluorescence Quantum Yields and Lifetimes.* The absorption and emission spectra of Rh3B were recorded in several solvents covering a large range of polarity and viscosity. A mirror image was obtained, which implies that the ground and excited states are similar. The maxima are collected in Table 1.

Radiative (k_f) and nonradiative (k_{nr}) rate constants were obtained, as usual, through the experimental fluorescence quantum yields (Φ_f) and lifetimes (τ_f) (eq 1a and eq 1b)

$$k_f = \Phi_f/\tau_f \tag{1a}$$

$$k_{nr} = 1/\tau_f - k_f \tag{1b}$$

The results obtained for the solvents studied are shown in Table 1. The values of the radiative rate constants do not vary significantly in agreement with the small Stokes shifts,[29] indicating similar charge distributions and geometries.[30] By

TABLE 1: Photophysical Data of Rh3B Cationic Form in Various Solvents at $T = 296$ K

solvent	label	λ_{abs} ±0.5/nm	λ_{em} ±0.5/nm	Φ_f ±0.05	τ_f ±0.05/ns	k_f ±0.1/10^8 s^{-1}	k_{nr} ±0.1/10^8 s^{-1}
methanol	1	555.4	577.5	0.45	1.94	2.3	2.8
ethanol	2	556.0	579.2	0.52	2.24	2.3	2.1
1-propanol	3	557.0	578.3	0.62	2.54	2.4	1.5
1-butanol	4	558.0	579.3	0.63	2.67	2.4	1.4
1-hexanol	5	558.6	582.1	0.66	2.89	2.3	1.2
1-decanol	6	559.2	580.5	0.73	3.26	2.2	0.8
2-propanol	7	556.0	579.2	0.56	2.28	2.5	1.9
2-butanol	8	556.8	578.8	0.67	2.77	2.4	1.2
2-methyl-2-propanol	9	557.0	579.4	0.66	2.50	2.6	1.4
cyclohexanol	10	561.0	582.5	0.82	3.26	2.5	0.6
water	11	558.6	583.9	0.28	1.49	1.9	4.8
1,2-ethanediol	12	561.8	584.0	0.53	2.71	2.0	1.7
1,3-propanediol	13	561.2	584.6	0.59	3.25	1.8	1.3
1,4-butanediol	14	562.0	582.7	0.75	3.34	2.2	0.7
1,5-pentanediol	15	561.0	583.0	0.74	3.41	2.2	0.8
tetraethyleneglycol	16	563.2	586.7	0.66	2.88	2.3	1.2
glycerol	17	563.4	586.6	0.85	3.49	2.4	0.4
acetonitrile	18	555.6	582.6	0.30	1.52	2.0	4.6
formamide	19	560.5	586.5	0.55	2.36	2.3	1.9
triacetine	20	560.0	583.9	0.73	3.19	2.3	0.8
propylene carbonate	21	559.0	585.0	0.48	2.13	2.3	2.4

contrast, the nonradiative rates vary largely with changes in the solvent properties.

The data obtained using monolinear alcohols, non-hydroxylated solvents, some branched alcohols, water and dihydric alcohols fall, respectively, in three parallel linear correlations between ln k_{nr} and ln η_s^0, the macroscopic shear viscosity (see Figure 2a). Deviations from the respective correlations are found for very viscous solvents such as cyclohexanol and glycerol. The slope extracted from these correlations with the rates obtained at constant temperature, is $\alpha = 0.4$, and is virtually the same as that found by other authors for Rhodamine B in alkanols, $\alpha = 0.38$.[31] The phenomenological nonradiative rate constants can then be described by eq 2 and as expected, linear correlations were also obtained, between ln k_{nr} and ln τ_L, the longitudinal dielectric relaxation time, as shown in Figure 2b.

$$k_s = \frac{A_S}{\eta^{\alpha}} \qquad (2)$$

3.2 Temperature Dependence. The use of eq 1a and 1b does not allow the separation of the activated from the nonactivated component, and the extracted k_{nr} value is the sum of all nonradiative processes. One way to overcome this difficulty is to calculate the activated part, $k_{nr}(T)$, from the total non radiative rate k_{nr}, using the value of the fluorescence lifetime (τ_{lt}) at a low enough temperature to cancel the contribution of the activated process. This method was adopted to obtain the activated part of the nonradiative rates, (eq 3),

$$k_{nr}(T) = \tau_f^{-1} - \tau_{lt}^{-1} \qquad (3)$$

from the temperature variation of the fluorescence lifetimes. Rh3B fluorescence lifetime in glycerol at 77 K was taken from the literature[15] and its inverse value used as τ_{lt}^{-1} (see footnote c) in Table 2). This value, ($\tau_{77K} = 3.88$ ns) was corrected[15] with the ratio of squared refractive indexes in each solvent and temperature to obtain, from the experimental fluorescence lifetime, the desired value of $k_{nr}(T)$. Typical fluorescence decays are shown in Figure 3, where a series of experiences illustrate the thermal deactivation of the dye fluorescence in 1,2-ethanediol. Using this procedure, Arrhenius plots (ln $k_{nr}(T) =$ ln $A - E_a/k_BT$) were constructed for the activated nonradiative rates, on the basis of lifetimes obtained from the convolution of a single-exponential function with the instrumental response of the Single Photon Counting apparatus (see Table 2).

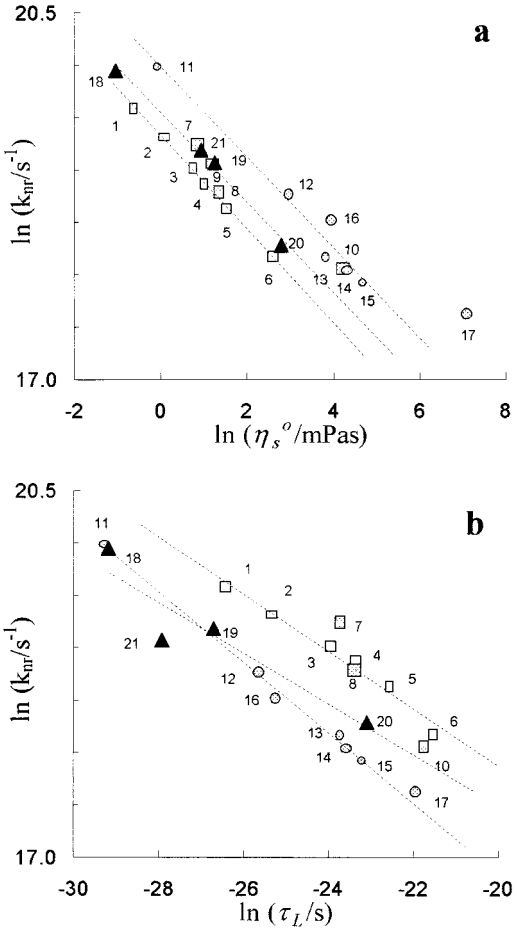

Figure 2. Correlations between the natural logarithm of the nonradiative rate constant k_{nr} ($T = 296$ K) of excited Rhodamine 3B cation and the natural logarithm of the (a) shear viscosity $\eta_s{}^o$; (b) longitudinal dielectric relaxation time. Legend: linear (1−6) and branched alkanols (7−10), (□); water (11) dihydric solvents (12−16) and glycerol (17), (○); non-hydroxylated solvents (18−21), (▲); trendlines: (- -).

TABLE 2: k_{nr} Arrhenius Parameters of First Excited Singlet of Rh3B Cationic Form

solvent	E_a (kJ mol^{-1})	A (10^{12} s^{-1})	ΔT^a (K)	N^b	r^2
methanol	22.08	2.53	271−306	7	0.996
ethanol	24.14	4.53	284−341	7	0.998
1-propanol	21.37	1.07	282−303	4	0.999
1-butanol	21.29	0.888	279−298	5	0.993
1-hexanol	23.00	1.37	286−330	8	0.998
1-decanol	28.32	6.90	287−331	6	0.994
2-butanol	20.24	0.540	282−328	7	0.999
cyclohexanol	25.97	2.40	296−329	7	0.981
water	25.20	13.3	282−350	6	0.999
1,2-ethanediol	30.74	36.9	282−316	5	0.999
1,3-propanediol	26.19	3.19	298−326	4	0.999
1,4-butanediol	29.39	9.73	296−330	5	0.991
1,5-pentanediol	27.99	5.04	296−329	5	0.997
tetraethyleneglycol	22.47	1.01	295−317	4	0.998
glycerol^c	41.42	487	280−349	17	0.996
acetonitrile	29.60	7.20	296−336	4	0.997
formamide	29.93	9.93	296−336	3	0.999
triacetine	29.18	4.70	283−342	9	0.994
propylene carbonate	23.91	3.96	286−336	5	0.999

^{a} Temperature range of the experimental fluorescence lifetime determinations. ^{b} Number of fluorescence decays taken in each solvent. ^{c} In this solvent, at the lower temperatures, the fluorescence lifetime approaches the limiting low-temperature lifetime. Due to this fact, the Arrhenius plot shows positive curvature. This enabled the estimation of the low-temperature value of the lifetime linearizing the plot by subtraction of an offset from experimental data using a least squares procedure. The calculation yielded the value $\langle\tau_{lt}\rangle = 3.83$ ns, in agreement with the literature value,[15] $\tau_{77K} = 3.88$ ns. The activation energy and preexponential factor presented for glycerol are thus obtained by the process described above.

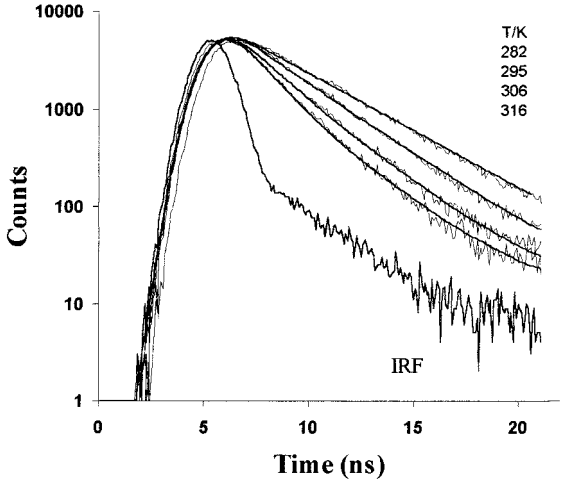

Figure 3. Fluorescence decays of Rhodamine 3B in 1,2-ethanediol as a function of temperature and instrumental response (IRF).

From the representative plots, shown in Figure 4, experimental activation energies were extracted which show little variation except for 1,2-ethanediol and glycerol (Table 2). The variation of the preexponential factor (A) also obtained from the Arrhenius representations is much more significant, showing that the main changes of $k_{nr}(T)$ are contained in these factors.

4. Modelization of Rate Constants. Kramers, in his seminal paper,[23] solved the equation for the motion of a particle subject to Brownian forces in a potential well and determined the rate of passage over a potential barrier considering the low, intermediate and high damping regimes. In the low damping case, the rate was found proportional to the solvent friction, becoming independent of it in the intermediate regime. The change between the low and intermediate damping regimes is

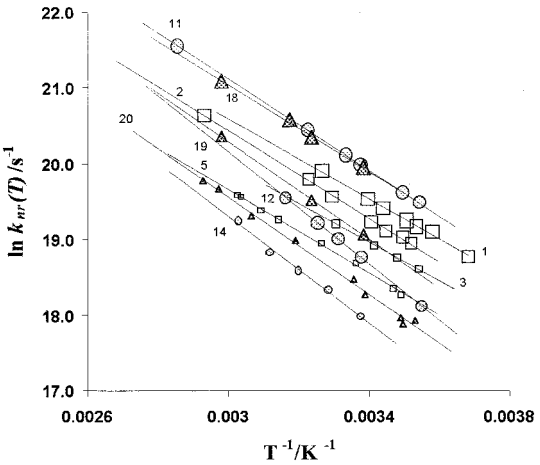

Figure 4. Arrhenius plots of the natural logarithm of the nonradiative rate constant $k_{nr}(T)$ of Rhodamine 3B excited first singlet state.

known as Kramers' turnover.[23,32] Kramers' expression for the rate in the intermediate and high friction (Smoluchowski limit) regimes is given by eq 4 (see Appendix 1).

$$k = \kappa_{Kr} k^{TST} \tag{4}$$

Kramers' transmission coefficient (κ_{Kr}) approaches unity in the intermediate friction regime where the reaction rate can be described by the Transition State Theory,[33] k^{TST} (eq 5). There, ω_0 represents the angular oscillation frequency of a parabolic reactant well and E_0 is the height of the potential barrier relative to the bottom of the well.

$$k^{TST} = \frac{\omega_0}{2\pi} e^{-E_0/k_B T} \tag{5}$$

In the Smoluchowski limit,[23] the phenomenological experimental rate constant can be described by eq 6 where the total friction, ζ, is affected by exponent α equal to unity and the parameter A_{exp} is friction independent. However, it is often found that $0 < \alpha < 1$ and then A_{exp} becomes friction dependent.

$$k_{exp} = \frac{A_{exp}}{\zeta^{\alpha}} e^{-E_a/k_B T} \tag{6}$$

The set of contributions that determine the nonradiative rates are due to an intrinsic barrier (E_0) and to frictional forces. However, it is not possible to evaluate directly the intrinsic barrier height. In fact, by plotting k_{nr} (T) with the temperature dependence in the Arrhenius equation

$$k_{nr}(T) = A e^{-E_a/k_B T} \tag{7}$$

the activation energy E_a is a sum of contributions related to the shear viscosity activation energy E_η and to the intrinsic barrier height $E_0(P)$ which is polarity dependent

$$E_a = \alpha E_\eta + E_0(P) \tag{8}$$

Introduction of eq 8 in eq 7 makes the result equivalent to eq 6 on the basis of three reasonable approximations: (1) the Arrhenian behavior of the zero frequency shear viscosity; (2) the power dependence on the viscosity does not depend on temperature; and (3) the temperature dependence of the intrinsic activation energy is considered negligible.

The rates of many reactions have shown, however, that the assumption of the Markovian limit is in general not adequate, being a rather particular case.[34] Grote and Hynes considered the effect of non-Markovian friction in the rate of passage over a parabolic barrier.[24] Their approach is able to account for dependencies weaker than the inverse power in the total friction. Their expression for the reaction rate, eq 9, corrects the Transition State rate through a transmission coefficient which is dependent on the barrier frequency ω_b and on the reactive frequency $\lambda_r = \kappa_{GH}\omega_b$ (see Appendix 1). The latter implicitly contains the memory effects of the frictional forces.

$$k = \kappa_{GH} k^{TST} \tag{9}$$

The theory of Grote and Hynes extends Kramers' intermediate and high damping result to the case of arbitrary frequency dependence on the friction coefficient. If the barrier frequency (ω_b) is low, the inverse dependence on the total friction is observed, whereas in the opposite case, when the barrier frequency approaches high values, the TST result is obtained.

Rather than following the procedure outlined in eq 6 to eq 8, our analysis was made by the direct application of Grote−Hynes theory[24] to the data.

The reaction was modeled with an unidimensional rotational coordinate affected by a polarity effect that comes from changes in charge distribution. If the contribution from the polarity may be regarded as static,[35] it is reflected only in the barrier height. In these conditions, it is possible to evaluate the friction contribution to the rate.

In the present work, we have used a procedure similar to the one described in the literature[36,37] for the calculations of the transmission coefficients (κ) in isomerization reactions. This parameter is obtained from the solution of the following equation, which is a rearrangement of Grote−Hynes expression for the transmission coefficient (see Appendix 1) for the reaction associated to a rotational motion

$$1 - \kappa^2 - \frac{\kappa}{I\omega_b}\hat{\zeta}(\kappa\omega_b) = 0 \tag{10}$$

where I is the moment of inertia. Equation 10, which leads to the determination of the transmission coefficient, was solved for each experimental temperature and for the range of unknown barrier frequency for the model solvents. The details of the calculation of the friction coefficient are discussed in Appendix 2.

The rotation of one diethyl amino group, which will correspond to isomerization at the C−N bond, was considered as a paradigm of conformational changes producing the activated nonradiative process. The mass of the rotating group was set to $m = 1.2 \times 10^{-25}$ kg. The radius R of the rotating sphere is set to 2.0 Å. The moment of inertia was set to $I = mR^2 = 4.8 \times 10^{-45}$ kg m^2.

Assuming that our experimental nonradiative rate $k_{nr}(T)$ can be described by k in eq 9, it is possible to obtain pairs (ω_o, E_o) for each calculated set of values of $\kappa(T)$ at a given ω_b, plotting the left part of eq 11 as a function of the reciprocal temperature.

$$\ln\left[\frac{k_{nr}(T)}{\kappa(T)}\right] = \ln\left(\frac{\omega_0}{2\pi}\right) - \frac{E_0}{k_B T} \tag{11}$$

Estimates of the two quantities appearing in eq 11 can be obtained from the intercept and slope. One important operational condition is, therefore, that the result of this representation gives a straight line. Another condition, to be fulfilled, is that the

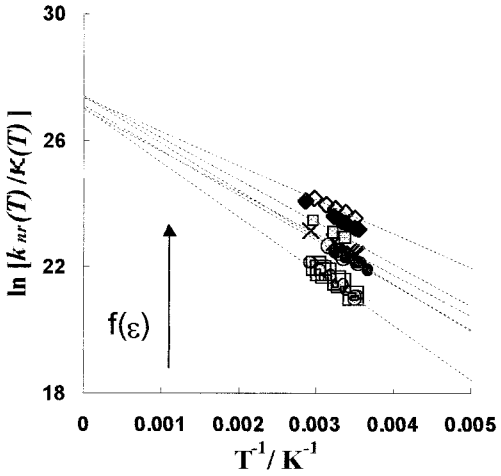

Figure 5. Estimates of the rate contants of the nonradiative deactivation of the first excited singlet state of Rhodamine 3B using eq 11. The values were calculated using the experimental results (Table 2) and the calculated κ (Appendixes 1 and 2). Symbols: see internal legend in Figure 7.

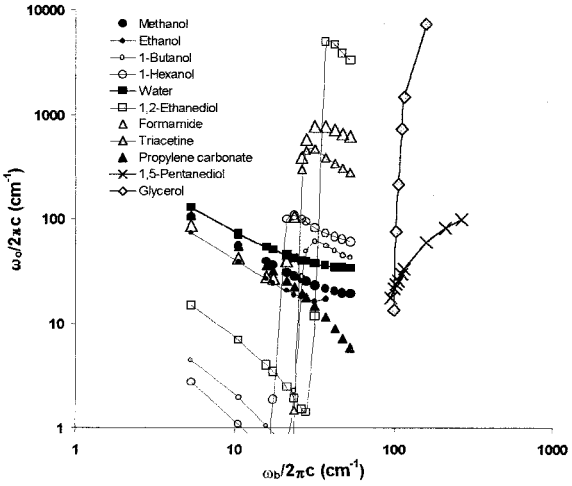

Figure 6. Representation of calculated reactant well wavenumbers ($\omega_0/2\pi c$) against barrier top imaginary wavenumbers ($\omega_b/2\pi c$) of Rhodamine 3B activated nonradiative rates.

(static) polarity dependence on the intrinsic barrier should be weak. (This is in agreement with the fact that no clear correlation with polarity functions could be obtained using the experimental activation energies.) One main difficulty resides in the fact that no estimates exist about possible reactant well frequencies (ω_o), barrier frequencies (ω_b), or intrinsic barrier heights (E_o). To overcome this problem the calculation of the transmission coefficients (κ), was done for a wide range of barrier frequencies ($10^{11} < \omega_b < 10^{14}$ rad s^{-1}). Using each experimental nonradiative rate and temperature, we have applied the treatment outlined to some representative solvents (monolinear alcohols, polyols, water, formamide, triacetine, and propylene carbonate).

The validity of our approach (eq 11) to obtain estimates of the Transition State Theory (TST) rates is illustrated in Figure 5. The results obtained for the values of the reactant well frequency at various values of the barrier frequency are shown in Figure 6 for the cases of water, methanol, ethanol, 1-propanol, 1-butanol, 1-hexanol, 1-decanol, 1,2-ethanediol, formamide, triacetine, and propylene carbonate (Table 3).

One observes that the wavenumbers corresponding to the reactant well oscillation when represented against the barrier top frequencies cross at a common value $\omega_0/2\pi c \cong \omega_b/2\pi c \cong 30$ cm^{-1}. The reactant well frequency does not change with

TABLE 3: Reaction Wavenumbers, Intrinsic Barrier Energies and Calculated Power Law Exponents for Solvents of Low Viscosity

solvent	$\omega_b/2\pi c$ (cm^{-1})	$\omega_0/2\pi c$ (cm^{-1})	E_0 (kJ mol^{-1})	$\alpha_\kappa = \frac{-\partial \ln \kappa}{\partial \ln \eta_s^0}$
methanol	26	26	12.4	0.931
ethanol	26	17	10.9	0.922
1-propanol	34	16	14.5	0.379
1-butanol	26	20	15.2	0.317
1-hexanol	19	18	14.3	0.381
1-decanol	16	40	15.2	0.449
water	24	42	10.9	0.932
1,2-ethanediol	32	20	11.8	0.648
triacetine	25	40	16.0	0.325
formamide	18	27	11.1	0.891
propylene carbonate	21	25	8.95	0.995

the solvent. This value may be a good approximation to the molecular mode involved in the nonradiative deactivation. In agreement with the assumption that there is weak polarity dependence, the barrier frequencies could be described by a common value in the different media.

4.1 Transmission Coefficients. The dynamic behavior exhibit changes from the Smoluchowski to the TST limit covering all solvents studied (see Figures 6, 7, and Table 3). In the framework of the model used, each liquid is characterized by a viscoelastic response (see Table A1, Appendix 2) which is felt in a given reactive time scale (roughly 1 ps, the inverse of the barrier frequency, ω_b). Solvents with high modulii, like water or propylene carbonate, have time to respond, whereas solvents such as propanol or triacetine respond more slowly. This allows that recrossings on the barrier top occur more frequently in the liquids whose viscoelastic response is faster.

The values obtained in two highly viscous media spanned by 1,5-pentanediol and glycerol are also given. Indeed, while in these solvents, $\omega_0/2\pi c$ is still 30 cm^{-1}, the imaginary barrier wavenumber ($\omega_b/2\pi c$) is 100 cm^{-1}. This value is higher than the one observed at the crossing region observed in Figure 6 for the lower viscosity solvents. Simultaneously, the transmission coefficients are higher and the dependence on zero frequency shear viscosity is weaker than the one found in the other cases.

4.2 Intrinsic Barrier Energies and Nature of the Transition State. Considering that the barrier height can be expressed by eq 12, the polarity dependent contribution may be related to the Onsager dipole interaction energy[38] in the following way:

$$E_0 = \Delta E_0^{vac} + \Delta W \qquad (12)$$

where the quantities in the right-hand side represent the energy differences of vacuum level and of dipole interaction energies of the barrier top relative to the bottom of the reactant well.

The intrinsic barrier energies calculated should correlate with the static dielectric constant Onsager function $f(\epsilon) = 2(\epsilon - 1)/(2\epsilon + 1)$. The lower energies are observed for the more polar solvents in the group. Changes in barrier heights obtained can be related to differences in the reaction fields felt by charge distributions at the bottom of the reactant well and at the barrier top. In Figure 8, the obtained[39] intrinsic barrier energies are plotted against the reaction field factor $f(\epsilon)$. From this analysis, a value of 42 ± 14 kJ mol^{-1} can be given as an estimate for the vacuum energy difference of the molecular conformations at the barrier top relative to the bottom of the reactant well. Depending on the cavity radius, a (assumed equal for both conformations), the difference of square values of the dipole moments can be estimated from the slope. Using $a = 4$ Å and

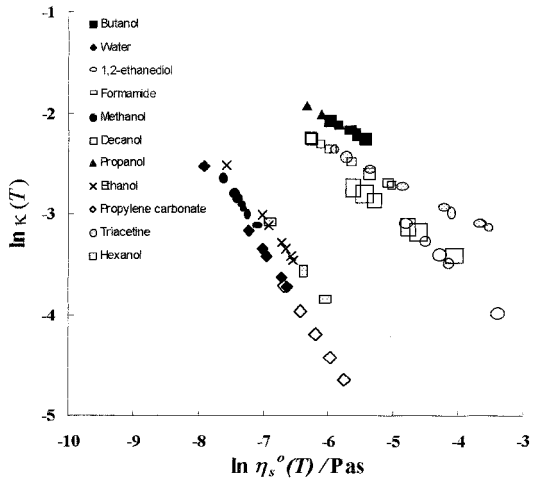

Figure 7. Correlation of calculated transmission coefficients, $\kappa(T)$ with the shear viscosity $\eta_s^o(T)$. The slopes (α_κ) are collected in Table 3 (last column). (For details see text).

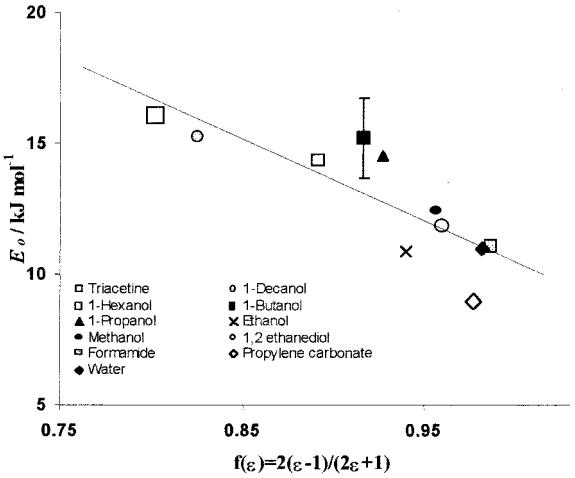

Figure 8. Correlation of intrinsic barrier energies (E_o) with Onsager reaction field factor of the static dielectric constant, $f(\epsilon)$. The error bar is calculated according to the assumption that the uncertainties[39] are from the experimental determinations only.

$\mu = 4.81$ D[40] for the first excited singlet, we obtain $\Delta\mu = 6 \pm 2$ D for the difference in dipole moment between the transition state conformation and the conformation at the bottom of the reactant well. In this interpretation, the increase of the transition state dipole moment relative to the reactant charge distribution can be viewed as an increase in the charge-transfer nature of the former.

In the cases of 1,5-pentanediol and glycerol, the calculated intrinsic barrier energies ($E_0 \cong 20$ kJ mol^{-1}) are significantly higher than the ones found for other solvents ($E_0 < 16$ kJ mol^{-1}) that can be grouped as displaying a common value of the reactant and barrier frequencies.

5. Discussion

The rates of isomerization in both the excited and ground electronic states usually follow a power law dependence with the solvent shear viscosity. For the molecules that are more frequently studied, e.g., stilbenes,[41] biphenyl butadiene,[42] and cyanine dyes,[42,43] this is indeed the case, and the same is found in previous studies on rhodamine excited-state dynamics.[15,18,22,31]

In our view, the lack of a unique correlation for all solvents is indicative that friction effects are felt differently by the reaction coordinate and that the intrinsic barrier height is also

changing. The results of our calculations show some evidence that there is separation of rates at constant temperature in different apparent correlations (Figure 2a). The reason is the balance between the static polarity effect and the frequency dependent friction since the barrier originates from conformational and charge distribution variations, whereas the frictional forces arise from the collisions with the solvent molecules during the reaction.

As pointed out by Vogel et al.[15] the slopes found in a given solvent from the temperature dependencies are different from the ones that are taken from the plots of variations of nonradiative rates when the solvent is changed. These differences may be interpreted in terms of different kinds of contributions to the process rate. When replacing one solvent by another, both polarity and viscosity are changed. Then, it is found that at different barrier heights the slope of the nonradiative rate dependence on the solvent viscosity is different in the case of the nonradiative deactivation of the fluorescence of Rhodamine molecules. This effect can be explained by the frequency dependent friction. Higher barriers are likely to be sharper than lower barriers. The lower imaginary frequencies will be found at the lower barriers leading to stronger dependencies on zero frequency shear viscosity. This is the central notion of Grote−Hynes theory,[24] which we believe is clearly reflected in the values obtained in this work. Indeed, they agree with each solvent viscoelastic response, using the friction model due to Zwanzig and Bixon[45] and Metiu, Oxtoby, and Freed,[46] and following the procedure of Bagchi and Oxtoby[36] and Rothenberger, Negus, and Hochstrasser[37] to account for the frequency dependence.

From our analysis, a definite value was obtained for the motion frequency at the bottom of the reactant well. Similar values were found[47] for torsion motions about the C−N bond in amino-aryl compounds.

The correlations with the dielectric relaxation times (τ_L) (see Figure 2b) allow us to infer that, besides the dynamic effects considered so far through the hydrodynamic study of the frictional contribution, there are still others related with the speed of dissipation from the solvation energy. For very viscous solvents such as 1,5-pentanediol and glycerol, no change is detected in the value found for the reactant well frequency, by contrast with the imaginary frequency at the barrier top, an observation which, by itself, also yields some information. This can be understood in terms of both static or dynamic (frequency dependent) contributions to the process of energy release in the solvent modes by the reaction coordinate, being compatible with changes in the reaction control. as observed previously with the transmission coefficients. The formulation of Grote−Hynes theory[24] used here assumes that the polarization field is always in equilibrium with the reaction coordinate. This assumption may not be fulfilled in the case of high viscous, slowly relaxing solvents. In very viscous solvents, such as 1,5-pentanediol or glycerol, the rate constant control may include a contribution from a different dynamic coordinate, probably related with the influence of nonequilibrium solvation in the course of the reaction. In this situation, it is possible that the reaction coordinate may become *bidimensional*, involving the solvent coordinate which will show non equilibrium polarization effects.[48,49] This hypothesis is consistent with the simultaneous charge-transfer process invoked in the nonradiative decay pathway, as will be reported in a forthcoming publication.[50]

6. Conclusion

The dynamic behavior of the thermally activated solvent dependent nonradiative rate constant for the decay of the first excited singlet state of Rhodamine 3B can be understood in terms of an isomerization process with changes in the geometrical coordinate. Grote−Hynes[24] theory was used to model the rotational coordinate participating in the nonradiative decay pathway.

The calculations lead to very similar frequencies in the reactant well and barrier top. The frequencies observed could be related to low frequency torsion modes compatible with the existence of frictional effects that actually determine the rate constants.

The charge-transfer nature of the transition state can be assigned in terms of a nonpolarizable dipole approximation to the reaction field factor.

Acknowledgment. This work was supported by Project PRAXIS/2/2.1/443//94. The authors are grateful to Professor J. T. Hynes for extensive and valuable discussions. Dr. C. A. M. Seidel, Dr. J. Karpiuk and Dr. V. Y. Artyukhov are also thanked for exchange of information. J.A.B.F. thanks PRAXIS XXI the financial support through Ph. D. grant BD/3616/94.

Appendix 1: Reaction transmission coefficients.

The Kramers transmission coefficient κ_{Kr}

$$\kappa_{Kr} = \left[1 + \left(\frac{\zeta}{2\omega_b}\right)^2\right]^{1/2} - \frac{\zeta}{2\omega_b} \tag{A1}$$

depends on the integrated friction expressed by eq A2 and on the frequency of the barrier, ω_b. In the high friction regime, the rate becomes inversely proportional to the friction. In this case, the friction exerted on the moving particle is the total (frequency independent) friction, ζ, (eq A2) which is proportional (in a hydrodynamic description) to the macroscopic shear viscosity, η_s^0 of the medium.

$$\zeta = \int_0^\infty \zeta(t)dt \tag{A2}$$

Grote−Hynes transmission coefficient κ_{GH} can formally be expressed in the same manner as κ_{Kr} and is defined by the following relation

$$\kappa_{GH} = \frac{\lambda_r}{\omega_b} = \frac{\omega_b}{\lambda_r + \int_0^\infty \zeta(t)e^{-\lambda_r t}dt} \tag{A3}$$

The effective frequency (p) dependent friction is thus the value of the Laplace transform of the time dependent friction, $\zeta(t)$, at the reactive frequency, λ_r.

Appendix 2: Friction Coefficients

The frequency *(p)* dependent friction coefficients, $\hat{\zeta}(p)$, were calculated according to the expression for noncoupled rotation of a sphere, which contains the mass of the rotating group. R is the sphere radius, and l is the distance from the center of the sphere to the axis of rotation[51] (eq A4).

$$\hat{\zeta}(p) = (R + l)^2\hat{\zeta}_{tr}(p) + \hat{\zeta}_r(p) \tag{A4}$$

The translational friction, $\hat{\zeta}_{tr}(p)$, is given by the expressions of Zwanzig and Bixon[45] and Metiu, Oxtoby and Freed,[46] (eq A5).

$$\hat{\zeta}_{tr}(p) = \frac{4\pi}{3}\eta_s(p)RX^2[2(X+1)P + (1+Y)Q] \tag{A5}$$

TABLE A1: Data Used in the Calculation of the Transmission Coefficients, $\kappa(T)$

solvent	$\eta_s^{o\,a,c}$ (10^{-3} Pas)	$\eta_v^{o\,a,c}$ (10^{-3}Pas)	$c_s^{a,c}$ (m s^{-1})	$\rho_o^{a,c}$ (kg m^{-3})	$G_\infty/10^8$ (Pa)	$K_r/10^8$ (Pa)
methanol	0.563	0.931	1152	790	59.6[m,b]	79.5[h,b]
ethanol	1.15	1.60	1165	789	8.47[h,b]	11.3[h,b]
1-propanol	2.08	2.44	1223	804	3.00[i,b]	4.00[i,b]
1-butanol	2.71	2.93	1268	810	1.62[h,b]	2.16[h,b]
1-hexanol	4.87	2.47	1310	816	0.886[h,b]	1.18[h,b]
1-decanol	11.9	6.37	1402	829	0.634[h,b]	0.845[h,b]
water	0.966	2.73	1489	998	97.0[d,b]	129[d,b]
1,2-ethanediol	17.5	9.1	1662	1109	2.82[e,b]	3.76[e,b]
1,5-pentanediol	123	81.9	988	987	5.94[f,c]	7.92[f,c]
glycerol	985	1073	1909	1101	23.3[g,c]	28.9[g,c]
triacetine	16.2	16.2	1382	1160	1.43[k,b]	10.6[k,b]
formamide	2.35	8.28	1644	1128	1.56[l,b]	8.21[l,b]
propylene carbonate	3.37	3.42	1438	1200	18.4[j,c]	24.5[j,c]

[a] Values at T=296 K. [b] Considered constant with temperature by nonavailability of data. [c] Considered temperature-dependent based on literature data. [d] Ref 55. [e] Calculated using data of ref 56. [f] Calculated using data of ref 57; Sound velocities for alcohols, ref 58; Bulk viscosities (alcohols), ref 59. [g] ref 59c. [h] Estimated using literature data from refs 56, 57, and 64. [i] Ref 56. [j] Ref 60. [k] Estimated using data from ref 61 [l] Ref 62. [m] Ref 63.

In addition, the frequency dependent rotational friction coefficient, $\hat{\zeta}_r(p)$, in the stick limit, is expressed by.[52]

$$\hat{\zeta}_r(p) = 8\pi\eta_s(p)R^3\frac{1 + X + \frac{1}{3}X^2}{1 + X} \tag{A6}$$

where

$$X = (p\rho_0/\eta_s)^{1/2}R;\ Y = p(c_s^{\,2} + p\eta_l/\rho_0)^{-1/2}R$$

$$P = \frac{3}{\Delta}(3 + 3Y + Y^2);\ Q = \frac{3}{\Delta}\left[3 + 3X + X^2 + \frac{X^2(1 + X)}{2 + \beta/\eta_s}\right] \tag{A7}$$

$$\Delta = 2X^2[3 + 3Y + Y^2] + Y^2[3 + 3X + X^2] + \frac{3X^2(1 + X)(2 + 2Y + Y^2)}{2 + \beta/\eta_s}$$

X and Y are wavevectors describing the propagation of the sound waves, η_s and η_l are, respectively, the shear and the longitudinal viscosities. ρ_0 is the solvent density, c_s is the velocity of sound and β is the slip parameter. β is fixed at 10^{10} Pa in all the calculations to account for the assumed stick boundary condition. The longitudinal (l), shear (s), and volume (v) viscosities are related by [53]

$$\eta_l(p) = \frac{4}{3}\eta_s(p) + \eta_v(p) \tag{A8}$$

The frequency dependence of the shear and volume viscosities were taken as Maxwell forms[54] with relaxation times inversely proportional to the elastic modulii of the respective relaxations (eq A9)

$$\eta_s(p) = \frac{\eta_s^0}{1 + p\tau_s};\ \eta_v(p) = \frac{\eta_v^0}{1 + p\tau_v}$$

$$\tau_s = \frac{\eta_s^0}{G_\infty};\ \tau_v = \frac{\eta_v^0}{K_r} \tag{A9}$$

The superscript 0 means a value at zero frequency. G_∞ is the infinite frequency shear modulus, and K_r is the relaxation part of the compression modulus.[53] The quantities present in all the preceding equations were allowed to vary with temperature when available experimental data exists. Some of the values used in the calculations are shown in Table A1.

Note Added after ASAP Posting:

This article was released ASAP on 12/5/2000 with minor errors in the equations and tables. The correct version was posted on 12/8/2000.

References and Notes

(1) (a) Drexhage, K. H. *Dye Lasers—Topics in Applied Physics*; Springer: Berlin, 1973; Vol. 1. (b) Drexhage, K. H. *J. Res. Nat. Bur. Stand.* **1976**, *80A*, 421.

(2) Batchelder, J. S.; Zewail, A. H.; Cole, T. *Appl. Optics* **1981**, *20*, 3733.

(3) (a) Sauer, M.; Han, K.-T.; Müller, R.; Nord, S.; Schulz, A.; Seeger, S.; Wolfrum, J.; Arden-Jacob, J.; Deltau, G.; Marx, N. J.; Zander, C.; Drexhage, K. H. *J. Fluoresc.* **1995**, *5*, 247. (b) R. P. Haugland, *Handbook of Fluorescent Probes and Research Chemicals*; Molecular Probes Inc.: Eugene, 1996. (c) Chen, L. B. *Annu. Rev. Cell. Biol.* **1988**, *4*, 155.

(4) Fries, J. R.; Brand, L.; Eggeling, C.; Köllner, M.; Seidel, C. A. M. *J. Phys. Chem. A* **1998**, *102*, 6601.

(5) Hinckley, D. A.; Seybold; P. G.; Borris, D. P. *Spectrochim. Act. A* **1986**, *42*, 747.

(6) Kemnitz, K.; Yoshihara, K. *J. Phys. Chem.* **1991**, *95*, 6095.

(7) Korobov, V. E.; Shubin, V. V.; Chibisov, A. K. *Chem. Phys. Lett.* **1977**, *45*, 498.

(8) Widengren, J.; Mets, Ü.; Rigler, R. *J. Phys. Chem.* **1995**, *99*, 13 368.

(9) (a) Barrigeletti, F. *Chem. Phys. Lett.* **1987**, 1*40*, 603. (b) Arden, J.; Deltau, G.; Huth, V.; Kringel, U.; Peros, D.; Drexhage, K. H. *J. Lumin.* **1991**, *48&49*, 352.

(10) (a) Bagchi, B.; Fleming, G. R.; Oxtoby, D. W. *J. Chem. Phys.* **1983**, *78*, 7375. (b) Bagchi, B.; Fleming, G. R. *J. Phys. Chem.* **1990**, *94*, 9.

(11) (a) Karstens, T.; Kobs, K. *J. Phys. Chem.* **1980**, *84*, 1871. (b) Kringel, U. *Thesis*, Siegen, 1988.

(12) (a) Zachariasse, K. A.; Grobys, M.; von der Haar, Th.; Hebecker, A.; Il'ichev, Yu. V.; Morawski, O.; Rückert, I.; Kühnle, W. *J. Photochem. Photobiol. A: Chem.* **1997**, *105*, 373.

(13) Grabowski, Z. R.; Rotkiewicz, K.; Rubaszewska, W.; Kirkor-Kaminska, E. *Act. Phys. Polon. A* **1978**, *54*, 767.

(14) Vogel, M.; Rettig, W.; Sens, R.; Drexhage, K. H. *Chem. Phys. Lett.* **1988**, *147*, 461.

(15) Vogel, M.; Rettig, W.; Sens, R.; Drexhage, K. H. *Chem. Phys. Lett.* **1988**, *147*, 452.

(16) Arbeloa, F. L.; Aguirresacona, I. U.; Arbeloa, I. L. *Chem. Phys.* **1989**, *130*, 371.

(17) Arbeloa, I. L.; Mukherjee, K. K. R. *Chem. Phys. Lett.* **1986**, *128*, 474.

(18) Arbeloa, I. L.; Mukherjee, K. K. R. *Chem. Phys. Lett.* **1986**, *129*, 607.

(19) Snare, M. J.; Treloar, F. E.; Ghiggino, K. P.; Thistlethwaite, P. J. *J. Photochem.* **1982**, *18*, 335.

(20) Huppert, D.; Kanety, H.; Kosower, E. M. *Faraday Dicuss.* **1982**, *74*, 11.

(21) Karpiuk, J.; Grabowski, Z. R.; De Schryver, F. C. *J. Phys. Chem.* **1994**, *98*, 3247.
(22) (a) Tredwell, C. J.; Osborne, A. D. *J. Chem. Soc., Faraday Trans. II* **1980**, *76*, 1627. (b) Osborne, A. D. *J. Chem. Soc., Faraday Trans. II* **1980**, *76*, 1638.
(23) Kramers, H. A. *Physica* **1940**, *7*, 284.
(24) Grote, R. F.; Hynes, J. T. *J. Chem. Phys.* **1980**, *73*, 2715.
(25) (a) Medeiros, G. M. M.; Leitão, M. F.; Costa, S. M. B. *J. Photochem. Photobiol. A: Chem.* **1993**, *72*, 255. (b) Ferreira, J. A. B.; Costa, S. M. B. *Chem. Phys. Lett.* **1999**, *307*, 139.
(26) Olmsted, J., III. *J. Phys. Chem.* **1979**, *83*, 2581.
(27) Parker, C. A. *Photoluminescence in Solution*; Elsevier: Amsterdam, 1968.
(28) O'Connor, D. V.; Phillips D. *Time-correlated single photon counting*; Academic Press: New York, 1984.
(29) (a) Renge, I. *J. Photochem. Photobiol. A: Chem.* **1992**, *69*, 135. (b) Renge, I. *Chem. Phys.* **1992**, *167*, 173.
(30) König, R.; Lau, A.; Weigmann, H.-J. *Chem. Phys. Lett.* **1980**, *69*, 87.
(31) (a) Casey, K. G.; Quitevis, E. L. *J. Phys. Chem.* **1988**, *92*, 6590. (b) Chang, T.-L.; Cheung, H. C. *J. Phys. Chem.* **1992**, *96*, 4874.
(32) Pollak, E.; Grabert, E.; Hänggi, P. *J. Chem. Phys*. **1989**, *91*, 4073.
(33) (a)Eyring, H. *J. Chem. Phys.* **1935**, *3*, 107. (b)Evans, M. G.; Polanyi, M. *Trans. Faraday Soc*. **1935**, *31*, 875.
(34) (a) Hynes, J. T. *J. Stat. Phys*. **1986**, *42*, 149 (b) Hänggi, P.; Talkner, P.; Borkovec, M. *Rev. Mod. Phys.* **1990**, *62*, 251.
(35) Hicks, J.; Vandersall, M.; Babarogic, Z.; Eisenthal, K. *Chem. Phys. Lett.* **1985**, *116*, 18.
(36) Bagchi, B.; Oxtoby, D. W. *J. Chem. Phys.* **1983**, *78*, 2735.
(37) Rothenberger, G.; Negus, D. K.; Hochstrasser, R. M. *J. Chem. Phys.* **1983**, *79*, 5360.
(38) Onsager, L. *J. Am. Chem. Soc.* **1936**, *58*, 1486.
(39) Benson, S. W. *The Foundations of Chemical Kinetics*; McGraw-Hill: New York, 1960.
(40) (a) Artyukhov, V. Y. *Sov. Phys. J.* **1986**, *29*, 534. (b) Artyukhov, V. Y. *Sov. Phys. J.* **1987**, *30*, 850.
(41) Waldeck, D. H. *Chem. Rev.* **1991**, *91*, 415.
(42) Mohrschladt, R.; Shroeder, J.; Troe, J.; Vhöringer, P. *J. Chem. Phys.* **1994**, *101*, 7566.
(43) Velsko, S. P.; Waldeck, D. H.; Fleming, G. R. *J. Chem. Phys.* **1983**, *78*, 249.
(44) (a) Åkesson, E.; Hakkarainen, A.; Laitinen, E.; Helenius, V.; Gilbro, T.; Korppi-Tommola, J.; Sundström, V. *J. Chem. Phys.* **1991**, *95*, 6508. (b) Korppi-Tommola, J. E. I.; Hakkarainen, A.; Hukka, T.; Subbi, J. *J. Phys. Chem.* **1991**, *95*, 8482.
(45) Zwanzig, R.; Bixon, M. *Phys. Rev. A* **1970**, *2*, 2005.
(46) Metiu, H.; Oxtoby, D. W.; Freed, K. F. *Phys. Rev. A* **1977**, *15*, 361.
(47) Phillips, D. *J. Photochem. Photobiol. A: Chem*. **1997**, *105*, 307.
(48) (a) van der Zwan, G.; Hynes, J. T.; *J. Chem. Phys.* **1982**, *76*, 2993. (b) van der Zwan, G.; Hynes, J. T.; *J. Chem. Phys.* **1983**, *78*, 4174.
(49) Kim, H. J.; Hynes, J. T. *J. Photochem. Photobiol. A: Chem*. **1997**, *105*, 337.
(50) Ferreira, J. A. B.; Costa, S. M. B. in preparation.
(51) Happel, J.; Brenner, H. *Low Reynolds Number Hydrodynamics*; Prentice Hall: Englewood Cliffs, 1965.
(52) Montgomery, J. A.; Berne, B. J. *J. Chem. Phys.* **1977**, *66*, 2770.
(53) Herzfeld, K. F.; Litovitz, T. A., *Absorption and Dispersion of Ultrasonic Waves*; Academic Press: New York, 1959.
(54) Maxwell, J. C. *Philos. Trans.* **1867**, *157*, 49.
(55) Bertolini, D.; Tani, A. *Phys. Rev. E* **1995**, *51*, 1091.
(56) Pinnow, D. A.; Candau, S. J.; Litovitz, T. A. *J. Chem. Phys.* **1968**, *49*, 347.
(57) Lampert, W.; Wang, C. H.; Fytas, G.; Dorfmüler, T. *J. Chem. Phys.* **1982**, *76*, 4872.
(58) (a) Marks, G. W. *J. Acoust. Soc. Am.* **1967**, *41*, 103. (b) *Handbook of Chemistry and Physics*, 72nd ed.; CRC Press: Boca Raton, 1991.
(59) (a) Markham, J. J.; Beyer, R. T.; Lindsay, R. B. *Rev. Mod. Phys.* **1951**, *23*, 353. (b) Hirai, N.; Eyring, H. *J. Appl. Phys.* **1958**, *29*, 810. (c) Meister, R.; Marhoeffer, C. J.; Sciamanda, R.; Cotter, L.; Litovitz, T. *J. Appl. Phys.* **1960**, *31*, 854.
(60) Ma, J.; Bout, D. V.; Berg, M. *J. Chem. Phys.* **1995**, *103*, 9146.
(61) Hashitani, R.; Hibi, M.; Koda, S.; Nomura, H. *J. Chem. Soc., Faraday Trans*. **1990**, *86*, 917.
(62) (a) Goodman, M. A.; Jain, V. K.; McKinnon, S. J., Whittenburg, S. L. *J. Phys. Chem.* **1986**, *91*, 1635. (b) Jordan, B. P., Sheppard, R. J.; Szwarnowski, S. *J. Phys. D. Appl. Phys.* **1978**, *11*, 695.
(63) Alonso, J.; Bermejo, F., J.; García-Hernández, M.; Martínez, J. L., Howells, W. S.; Criado, A. *J. Chem. Phys.* **1992**, *96*, 7696.
(64) Champion, J. V.; Jackson, D. A. *Mol. Phys.* **1976**, *31*, 1159.